Morphology of coronal hole based on SDO/AIA data in May 2010 - December 2013

Filip Šterc[1], Darije Maričić[1]and Dragan Roša[1]

[1] Zagreb Astronomical Observatory, Opatička 22, 10000 Zagreb, Croatia.

Abstract.

We present an analysis of the high speed streams (HSSs) parameters, using *in situ* WIND data recorded from May 2010 to December 2012. For this purpose we made a list of 202 solar wind disturbances incorporated into an online catalogue for general use. Separating the solar wind signatures on: high speed streams, interplanetary coronal mass ejections (ICMEs), complex signatures; we focused our attention on 102 HSSs (52% of all SW signatures) which can be clearly associated with particular stream interface (SI). Furthermore, we analyzed in detail the correlation of solar wind parameters in different parts of HSSs, particularly in front and behind of SI. We found the best correlation between maximum of the magnetic field strength *Bvs* proton density *N*p and proton thermal speed v_{th}, 0.65 and 0.62, respectively. As well as between flow speed *v* and proton thermal speed v_{th}, cc = 0.64. While the correlation is significantly lower (cc = 0.38) between magnetic field *B* and flow speed *v.* Also, the correlation between maximum of the magnetic field *B*, flow speed *v* and proton thermal speed v_{th}, in the regions of HSS before and after SI are: cc = 0.84, 0.66 and 0.79, respectively. Correlations for the maximum of the proton density *N*p between these two HSS regions is significantly lower (cc = 0.39) and points out to the possibility of two different HSS families.

Keywords. solar wind disturbance, stream interface, high speed stream

Introduction

Corotating interaction regions (CIRs) are created by the interaction of the high speed solar wind streams (HSSs) and slow solar wind streams (e.g., *Tsuratani et al.,* 2006, and references therein). The slow solar wind speed has a typical speed from 300 to 400 kms^{-1}, while the high-speed solar wind may reach velocities up to 800 kms^{-1}. CIRs originate from a coronal hole on the Sun (*Krieger, Timothy and Roelof*, 1973) and cause recurrent activity in the interplanetary space (e.g. *Gosling,* 1996). Furthermore, at heliocentric distance of around 1 AU, CIRs are usually bounded by magnetohydrodinamic forward and reverse waves, which develop into a forward and reverse shocks at a larger distance, occasionally some events develop already at 1 AU (*Smith and Wolfe,* 1976). CIRs cause geomagnetic storms of medium to weak strenghts (e.g. *Vennerstorm,* 2001; *Verbanec et al.,* 2011a,b; *Hajra et al.,* 2013, *Vršnak*

et al., 2017), although this phenomena is much stronger when it is caused by a single ICME or ICMEs interaction. CIRs occur more common throughout the solar cycle and their cumulative effect is larger than those of ICMEs (*Tsuratani et al.,* 2006). From the measurements of the solar wind at 1 AU, a CIR structure is characterized by the compression region associated with stream interface (SI). Inside the compression region the magnetic field, the temperature and the plasma density are increased (*Dumbović et al.*, 2012, and references therein). Compression region usually lasts typically one day. The whole region contains strong fluctuation and the increase of the southward-directed magnetic field is always present. Fast HSS from coronal holes lasts typically several days and reach flow speeds that can reach values above 800 kms^{-1}. For the evolution and structure of CIRs see articles *Baloghet al.,* 1999 as well as *Gosling and Pizzo,* 1999. The main objective of the analysis presented in this article is the comparison of measured magnetic field and plasma SW parameters in different parts of the CIR. In following Section 2 we describe the data used for our study. Section 3 describes data analysis of the magnetic field and plasma parameters in different parts of HSS, that were recorded by *in situ* measurements at the Langrangian point L1, focusing on the period from May 2010 to December 2012. In particular, we analyze, in detail, the relationship between: the magnetic field, B; the flow speed, v; the thermal proton speed, v_{th}; and proton density, Np, in front and behind the SI. The main results and conclusions of the research are summarized and discussed in Section 4.

The data set

For the measuring of solar wind disturbances at L1 point we used the data recorded by the Magnetic Field Investigation (MFI) and Solar Wind Experiment (SWE) Wind instruments (http://wind.nasa.gov/mfi_swe_plot.php), with 1 minute resolution data in GSE coordinates. The HSS events were separated by a detailed analysis of plasma and the magnetic field structure, as described in *Dumbović et al.* 2012. First we identified the increase of the plasma speed above the current background wind speed level, which corresponds to high-speed streams (for details see *Vršnak, Temmer, and Veronig,* 2007a). Also, we found the compression region or SI at the rising phase of the HSS from the data of plasma temperature, density and magnetic field (a sharp peak of the density and field strength, as well as sharp increase of temperature). Using the IS we separated the HSS on two parts. The *in situ* data in Figure 1 show that the structure of the HSS consists of two different parts (separated by the vertical dashed lines). Middle vertical dashed line represents stream interface. In both parts we measured the magnetic field strength, change in GSE magnetic field components, flow speed, maximum and minimum values of the flow speed components, temperature, proton density and plasma-to-magnetic field pressure (β). First region, which we marked with 0 (part of the HSS form onset of HSS to the onset SI) is characterized by a gradual increase of magnetic field strength, decrease in temperature and strong increase of proton density. The second region, which we marked with the number 1 (part of the HSS from the onset of SI to the end of the HSS)

is characterized by a sharp drop of proton density, increased magnetic field strength, flow speed and temperature.

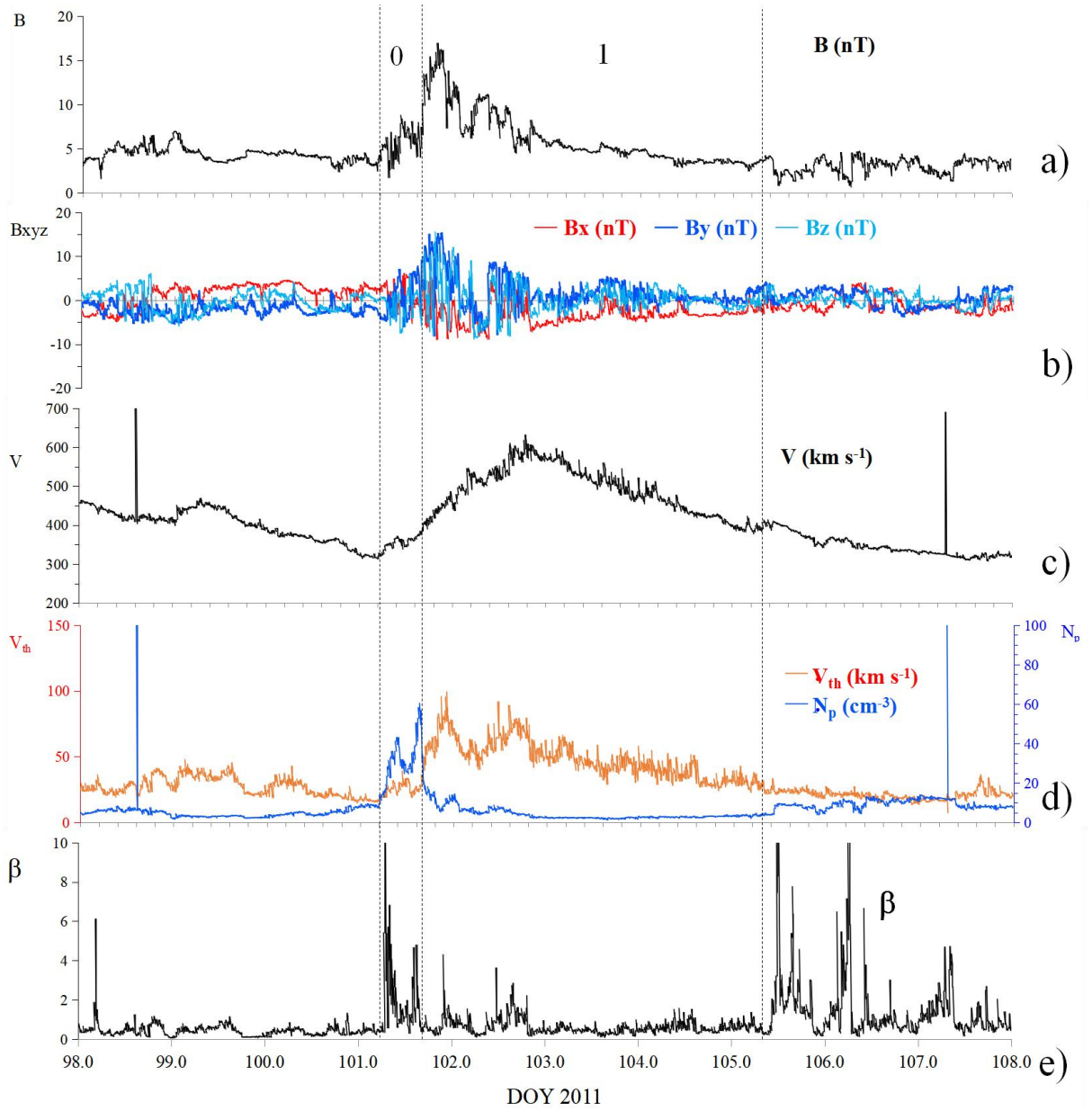

Figure 1. The presented figures the following labels are: a) the magnetic field strength, b) GSE magnetic field components, c) solar-wind speed, d) proton density and thermal velocity and e) plasma-to-magnetic pressure ratio. From a) to e): Example of the HSS in situ WIND measurements at L1 (DOY (day of year) = 98 is 8April 2011). This HSS, measured by WIND satellite occurred on 13 April 2011, represents events with clearly distinctive features of SI (middle dashed vertical line). The morphology of such HSS can be divided into two different parts: part of the HSS between the front wave and SI (which is marked with number 0) and part of the HSS between SI and reverse wave (which is marked with number 1). First and last vertical dashed lines represent forward and reverse waves, while the middle dashed lines represent stream interfaces or interaction region.

As the end of HSS we took the time when the flow speed returned to the same values, as on the onset ot the speed increase. In Figure 1; in every plot the date is expressed as DOY.

For the analyzed period, from 202 solar wind disturbances, 137 have been recognized as HSSs (67% of all SW samples). From the whole HSS sample, 74% of HSSs show a typical field and plasma structure and SI inside the CIR which can be clearly recognized. Between 137 HSS events, 35 events (25% of whole CIR sample) have complex signatures, and have been defined as events with complex signatures. For such HSSs it was not possible to clearly recognize the SI, but it was possible to recognize two or more SI, which can be caused by HSSs or ICME-HSS interaction. These events are excluded from our analysis. Our list of HSS events can be found at https://zvjezdarnica.hr/pdf/ListSWDs2010.pdf. For each HSS we provide the following information: no. of event (column 1); date of HSS disturbance (column 2 - 4); column 5 - 7 give information whether the HSS is associated with a change in cosmic ray neutron flux, Dst index and whether is shows a rotation of the magnetic field. For the purpose of this analysis we separated the SWDs into different types: ICMEs, HSSs and complex signatures, and the SWD type is noted in column 8; in columns 9 - 16 we give information on the SWD onset and the maximum values of magnetic field strength and plasma parameters; finally columns 17 - 19 give information about the onset and values of change, maximum and minimum of the Dst index.

Analysis

The results presented in this section quantify the previously described behaviour in statistical sense concerning the analysed period (from May 2010 to December 2014), are presented in graphical form in Figures 2 and 3. The correlations between four HSS-related solar wind parameters measured by *in situ* WIND data, are shown in Figure 2a-d. The presented scatter plots relating the correlation between the maximum measured values of the solar wind magnetic field strength B, proton density Np, flow speed $v$and proton thermal speed v_{th}, over the analyzed period. The graphs reveal a well defined lower and upper limits to v (B), Np (B), v_{th} (B) and v_{th} (v), indicated by the dotted line. In every graph we displayed the linear last-squares fit for solar wind parameters related data. We found the best correlations, cc = 0.65, 0.62 and 0.64, between: proton density and magnetic field strength, proton thermal speed and magnetic field strength, as well as proton thermal speed and flow speed, respectively. While a significant lower correlation cc = 0.38 was found between the flow speed and magnetic field strength.

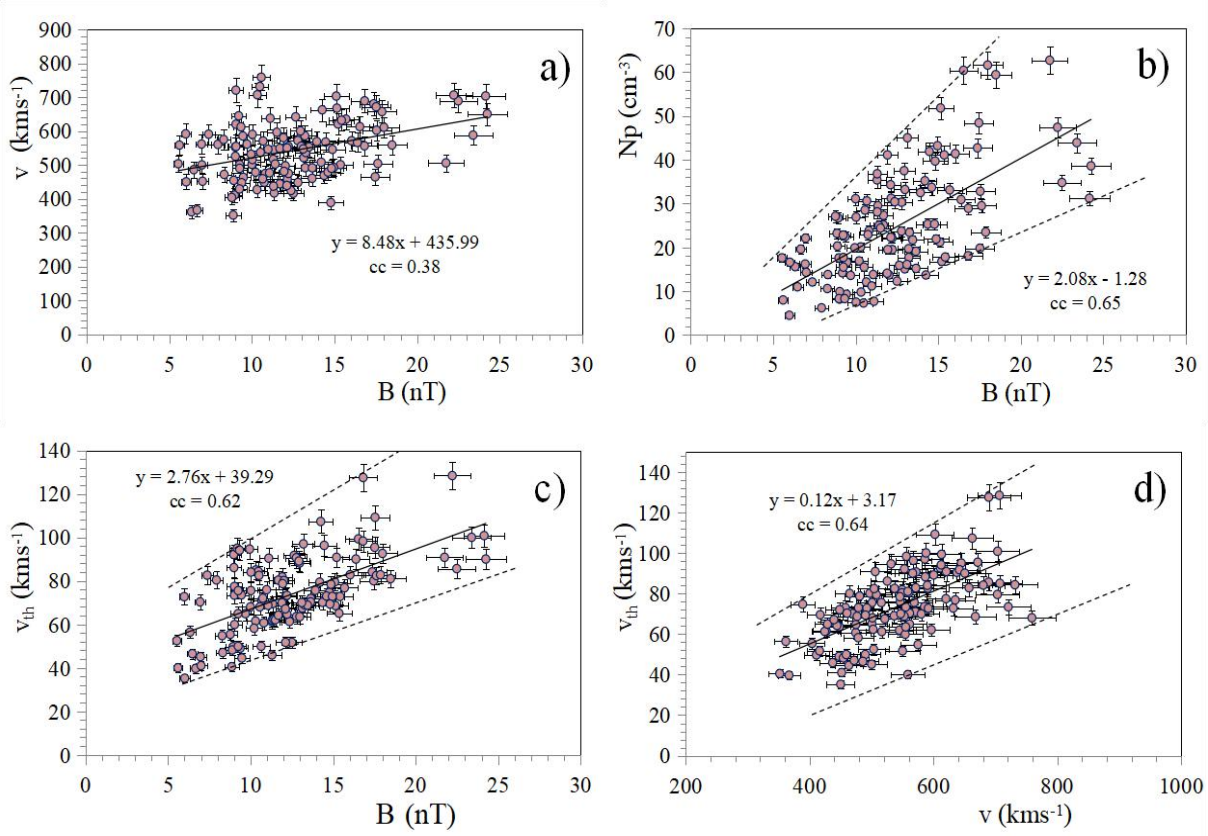

Figure 2. The following labels are: a) flow speed vs magnetic field strength, b) proton density vs magnetic field strength, c) thermal velocity vs magnetic field strength, and d) thermal velocity vs solar-wind speed. Dashed line represents a provisional drawn possible lower and heights values for the specific solar wind parameter.

In Figures 3a-d we plotted the variation of the four solar wind parameters measured separately in two different parts of the HSS for the same analyzed period (noted as parts 0 and 1 in the Figure 1). There is a high correlation between the maximum of magnetic field strength B, solar wind flow speed and proton thermal speed in HSS parts 0 and 1, with correction coefficients of cc = 0.84, 0.66 and 0.79, respectively.

While, a very weak correlation (cc = 0.39) was found between maximum values of the proton density *N*pmeasured in regions 0 and 1. Inspecting the graphs (Figure 3b), we can distinguish that the variation between maximum of the proton density in HSS parts 0 and 1 show two different correlations or possible two different families of the HSS.

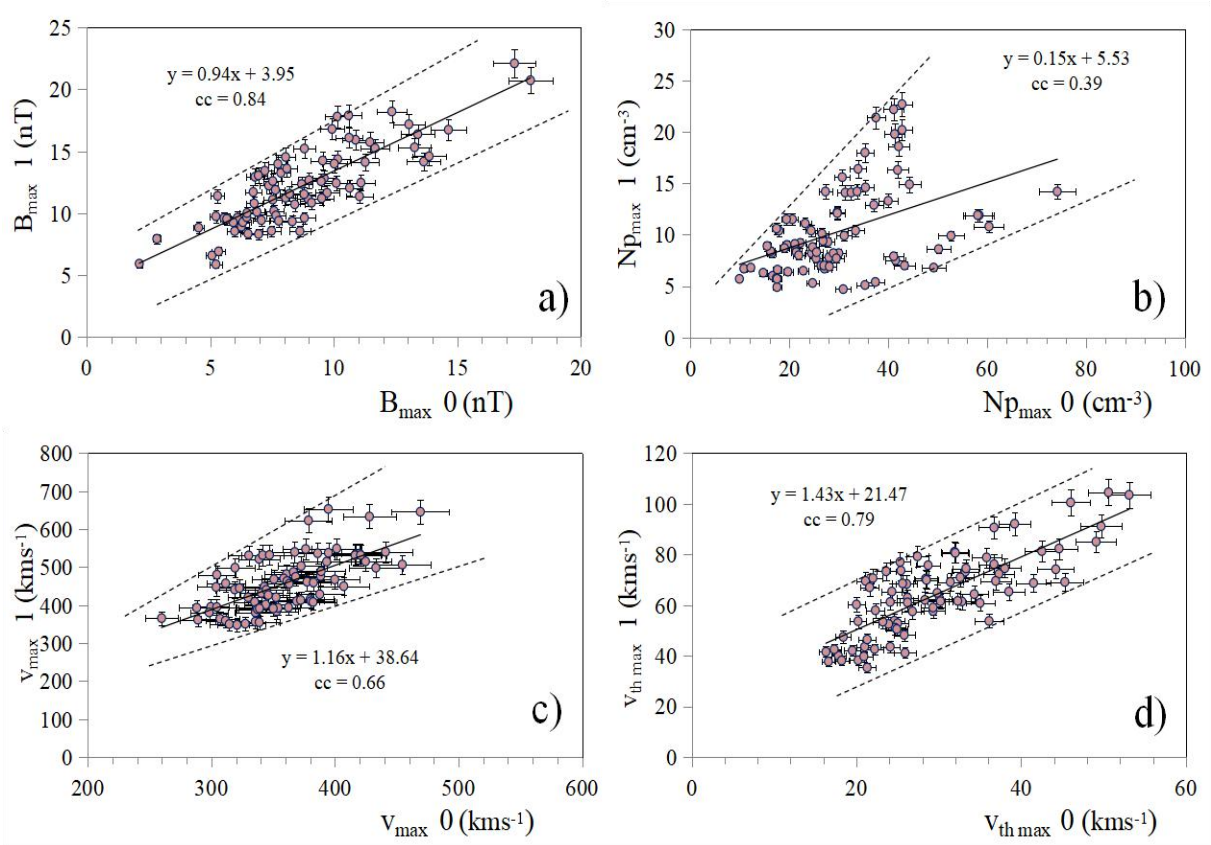

Figure 3. Variation between maximum of: a) magnetic field strength B b) proton densityc) solar wind flow speed and d) proton thermal speed, in HSS parts 0 and 1. The dashed line represents a provisionaly lower and higher values for the specific solar wind parameter.

Discussion and Conclusion

We summarize the main results of our analysis of the HSS-related solar wind parameters as follows:

a) For our analyzed sample of the SWDs, 52% of the whole solar wind disturbances can be recognized as a HSS, which can be clearly associated with a particular stream interface.

b) We found high correlations between maximum of the magnetic field strength *Bvs* proton density *N*p and proton thermal speed v_{th}, as well as between flow speed *v* and proton thermal speed v_{th}, with correlation coefficients 0.65, 0.62 and 0.64, respectively. While the correlation is significantly lower (cc = 0.38) between magnetic field *B*and flow speed *v*.

c) Correlation between the maximum of the magnetic field *B*, flow speed *v* and proton thermal speed v_{th}, in the regions of HSS behind and after SI are: cc = 0.84, 0.66 and 0.79, respectively. Correlations for maximum of the proton density *N*p between these two HSS regions is significantly lower (cc= 0.39) and points out to a possibility of two different HSS families.

We would like to thank the WIND, ACE, SOHO, STEREO, SDO and Kyoto University teams for developing and operating the instruments and we are grateful for their open data policy.

References

Balogh, A., Gosling, J.T., Jokipii, J.R., Kallenbach, R., Kunow, H. (1999). Corotating interaction regions.*Space Sci. Rev.* **89**, 1.

Dumbović, M., Vršnak, B., Čalogović, J., Župan, R. (2012). Cosmic ray modulation by different types of solarwind disturbances. *Astron. Astrophys.* **538**, A28.

Gosling, J.T. (1996). Corotating and transient solar wind flows in three dimensions. *Annu. Rev. Astron. Astrophys.***34**, 35.

Gosling, J.T., Pizzo, V.J.: (1999). Formation and evolution of corotating interaction regions and their threedimensional structure. *Space Sci. Rev.* **89**, 21.

Hajra, R., Echer, E., Tsurutani, B.T., Gonzalez, W.D. (2013). Solar cycle dependence of high-intensity longd uration continuous AE activity (HILDCAA) events, relativistic electron predictors? *J. Geophys. Res.***118**, 5626.

Krieger, A.S., Timothy, A.F., Roelof, E.C. (1973). A coronal hole and its identification as the source of a high velocity solar wind stream. *Solar Phys.***29**, 505.Smith, E.J., Wolfe, J.H. (1976). Observations of interaction regions and corotating shocksbetween one andfive AU – Pioneers 10 and 11. *Geophys. Res. Lett.* **3**, 137.

Tsurutani, B.T., McPherron, R.L., Gonzalez, W.D., Lu, G., Sobral, J.H.A., Gopalswamy, N. (2006). Introductionto special section on corotating solar wind streams and recurrent geomagnetic activity. *J. Geophys.Res.* **111**, 1.

Vennerstroem, S. (2001). Interplanetary sources of magnetic storms: a statistical study. *J. Geophys. Res.* **106**, 29175.

Verbanac, G., Vršnak, B., Veronig, A., Temmer, M. (2011a). Equatorial coronal holes, solar wind high-speedstreams, and their geoeffectiveness. *Astron. Astrophys.* **526**, A20.

Verbanac, G., Vršnak, B., Živković, S., Hojsak, T., Veronig, A.M., Temmer, M. (2011b). Solar wind high-speedstreams and related geomagnetic activity in the declining phase of solar cycle 23. *Astron. Astrophys.* **533**,A49.

Vršnak, B., Temmer, M., Veronig, A.M. (2007a). Coronal holes and solar wind high-speed streams: I. Forecastingthe solar wind parameters. *Solar Phys.* **240**, 315.

Vršnak, B., Dumbović, M., Čalogović, J., Verbanec, G., Poljanić-Beljan, I. (2017). Geomagnetic Effects of Corotating Interaction Region. *Solar Phys.* **292**, 140.